

Drivers, Detection, and Impacts of Precipitation from the Radiation Belts

C. J. Rodger¹, M. A. Clilverd², W. Li³, M. P. McCarthy⁴, Y. Omura⁵, and C. E. Weaver⁶

¹ Department of Physics, University of Otago
Dunedin, New Zealand
email: crodger@physics.otago.ac.nz

² British Antarctic Survey (NERC)
Cambridge, United Kingdom
email: macl@bas.ac.uk

³ Atmospheric and Oceanic Sciences, UCLA,
Los Angeles, CA, USA
email: moonli@atmos.ucla.edu

⁴ Department of Earth and Space Sciences,
University of Washington, Seattle, USA
email: mccarthy@ess.washington.edu

⁵ Research Institute for Sustainable Humanosphere, Kyoto University,
Kyoto, Japan.
email: omura@rish.kyoto-u.ac.jp

⁶ University of Calgary, Calgary,
Canada
email: carol.weaver@unh.edu

Abstract

Particle precipitation into the atmosphere is believed to be one of the dominant mechanisms for the loss of energetic electrons from the Van Allen radiation belts. Wave-particle interactions involving ULF through to VLF waves are thought to be important drivers of these loss-events. There is growing interest in Energetic Electron Precipitation (EEP). Much of the renewed interest comes from NASA's recent Van Allen Probes mission, which has stimulated new experimental and theoretical research and opened up new understanding into the fundamental physical processes of radiation belt dynamics. There is also a new focus on the impact of the EEP on the polar atmosphere, with increasing evidence of significant changes in upper atmospheric chemistry and coupling to polar surface climate.

Background Information

Earth is surrounded by regions of magnetospherically trapped high energy particles, with intense fluxes of relativistic energy electrons (>1 MeV). These regions are known as the inner and outer Van Allen radiation belts, named after their discoverer James A. Van Allen of the University of Iowa. The first observations of the Van Allen belts date back to the very beginning of the Space Age, undertaken by Explorer-1 and Explorer-3 in early 1958 as part of the International Geophysical Year. This was unexpected, with the early observations prompting one of Van Allen's research team to proclaim "My God, Space is Radioactive". A schematic showing the basic location of the radiation belts relative to the Earth and inner magnetosphere is shown in Figure 1.

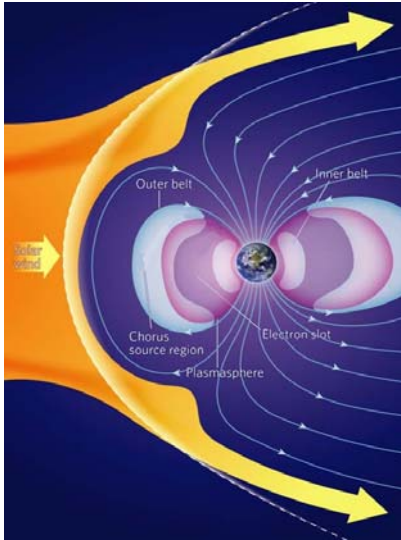


Figure 1. A schematic view of "Geospace", that region of space closest to the Earth which includes the Van Allen Radiation Belts and dominated by the geomagnetic field. Image adapted from [1].

As most satellites spend their lives inside the radiation belts, they are directly affected by this environment. Earth-orbiting satellites can be damaged or even lost due to increased high-energy electron fluxes in the Earth's radiation belts. In particular, the outer radiation belt (located 3.5-8 Earth radii from the Earth's centre) is highly dynamic with fluxes changing by a factor as large as 1000 on timescales of hours to days. These changes are triggered by processes originating from the Sun, and in particular by fluctuations in the solar wind, themselves reflecting conditions in the Sun's outer atmosphere. While originally discovered in the dawn of the space-age, there are still significant questions surrounding the relativistic electrons in the radiation belts. Many scientists around the world are investigating how the flux of outer radiation belt electrons can change by so much, and so quickly.

The upcoming URSI General Assembly and Scientific Symposium (Beijing, PRC, 16-23 August 2014) features two sessions directly focused on the energetic radiation belts (H01: Wave-Particle Interactions and Their Effects on Planetary Radiation Belts and HG03: Drivers, Detection, and Ionospheric Impacts of Precipitation from the Radiation Belts), as well as Commission H's tutorial by Professor Yoshiharu Omura of Kyoto University (Theory and simulations of nonlinear wave-particle interactions in the planetary radiation belts). The session descriptions for the two sessions are copied below:

H01/02/03/05 description: Wave-particle interactions are a ubiquitous physical phenomenon that allows the exchange of energy and momentum between natural plasma waves, and energetic radiation belt particles. In so doing, the wave can act as an energy conduit between different particle energies, species, or both. In this session we discuss the various plasma waves that control planetary radiation belt dynamics, their specific effects on the particles, both individually and in concert, and the various modes of wave-particle interactions, for instance linear, quasi-linear, nonlinear and non-resonant. We welcome both theoretical and observational studies involving the radiation belts of the Earth or other planets. We particularly encourage early results from the Van Allen Probes. Note that studies directed towards radiation belt particle precipitation and its effects are likely better suited to the complementary session HG1.

HG03/04 description: Particle precipitation into the atmosphere is believed to be one of the dominant mechanisms for the energetic electron loss from the Van Allen radiation belts, as well as ring current ions. Wave-particle interactions with ULF through to VLF waves are thought to be important drivers of these loss-events. This session is targeted at both ground-based and satellite experimental observations, as well as theoretical investigations, into the precipitation of energetic (>20 keV) and relativistic electrons or ring current ions. Papers considering wave-particle interactions driving losses, measurement of loss fluxes, or the effects of this precipitation on the ionosphere are welcome. We particularly welcome early results from the Van Allen Probes, the BARREL campaign, or studies

from existing ground and space based experiments. Note that studies directed towards radiation belt electron acceleration or transport are likely better suited to the complementary session H1.

In this Radio Science Bulletin paper we report on the growing interest in Energetic Electron Precipitation (EEP) from the Van Allen radiation belts, which has led to the HG03 session in the upcoming GASS. This is an area in which electromagnetic waves are core to all the physical mechanisms of acceleration, transport and loss of radiation belt energetic electrons. In addition, multiple experimental techniques have been employed to monitor the occurrence and properties of EEP as it strikes the ionosphere. These tend to rely either upon the energy released (by measuring X-rays, for example by high altitude balloons) or by monitoring the electrical conductivity of the upper atmosphere which is increased by EEP (and sensed by waves ranging from over frequencies from VLF through to the L-band employed by GNSS in Total Electron Content measurements). We include information from each one of the invited speakers from the HG03 session, as well as where EEP fits into the wider scientific picture.

Wave-Particle Interactions

Wave-particle interactions are a ubiquitous physical phenomenon that allows the exchange of energy and momentum between natural plasma waves, and energetic radiation belt particles. In so doing, the wave can act as an energy conduit between different particle energies, species, or both. The basic physics of the propagation of these waves through the magneto-active plasma leads the waves to be circularly polarized. For waves in the VLF range, the polarization is right-hand circular. This has become known as the "whistler mode", as one of the most common forms are whistlers, caused by the electromagnetic waves from lightning propagating through the plasma. A number of naturally occurring whistler-mode waves exist, with chorus and hiss being examples with high importance to the radiation belts. The whistler mode is sometimes referred to as the electron cyclotron mode, as it has the same "sense" as an electron gyrating in a magnetic field. In the ULF-ELF range, the waves propagation is left-hand circularly polarized, commonly termed the ion cyclotron mode (which assumes a positively charged ion). An example of these waves are Electromagnetic Ion Cyclotron Mode (EMIC) waves, which are also important in radiation belt dynamics.

As the whistler and ion-cyclotron mode waves are circularly polarized, they may resonate with the gyrating electrons and ions found within the Van Allen Radiation Belts. So called "Normal" resonance occurs between the doppler shifted wave and the particle, with electrons resonating with whistler mode waves and protons with ion cyclotron mode waves (Figure 2). The interactions between an electron and a right hand polarized wave depends on the energy of the electron, such that there are relativistic considerations. If $\gamma < \Omega_c/\omega$, the wave and particle propagate in opposite directions as in Figure 2 (i.e., counter-streaming), where γ is the Lorentz factor, Ω_c is the angular cyclotron frequency and ω is the angular wave frequency. However, if the particle energy is still higher, such that $\gamma > \Omega_c/\omega$, the wave and particle will move in the same direction. While this is still normal cyclotron resonance, the electron does not overtake the wave packet, because $V_R < V_p < V_g$ (for $\omega < 0.5 \Omega_c$), where V_R is the particles resonance velocity, V_p is the wave phase velocity and V_g is the wave group velocity.

These wave-particle interactions lead to the exchange of energy and momentum, which can amplify or attenuate the wave, with a corresponding momentum change in the particle and/or a change in the vector quantity, leading to pitch angle scattering. It is important to note that so called anomalous, or "parasitic resonances" [2], can also occur particularly when a particle overtakes a circularly polarized wave. This is possible for relativistic particles, and waves travelling at comparatively low speeds due to the refractive index of the plasma. An example of this is the interaction between relativistic electrons and EMIC waves, where the over-taking electron sees the EMIC wave as being right-hand circularly polarized.

During geomagnetic storms, both VLF and ULF waves are enhanced, which in turn, can enhance the transport of electrons within the outer radiation belt and also drive wave-particle interactions between energetic electrons and magnetospheric waves. Here "transport" refers to radial diffusion, which occurs as a result of drift-resonance between ULF waves and the drifting electrons. These interactions are known to accelerate electrons from seed populations of ~30 keV to energies of >1 MeV while at the same time perturbing a fraction of the trapped population onto paths which are likely to interact with the Earth's atmosphere [3]. Electrons which magnetically mirror at altitudes that are so low that they will hit the neutral atmosphere and be lost are said to be in the bounce-loss cone, precipitating into the atmosphere at ~100 km altitude.

(Normal) Cyclotron Resonance

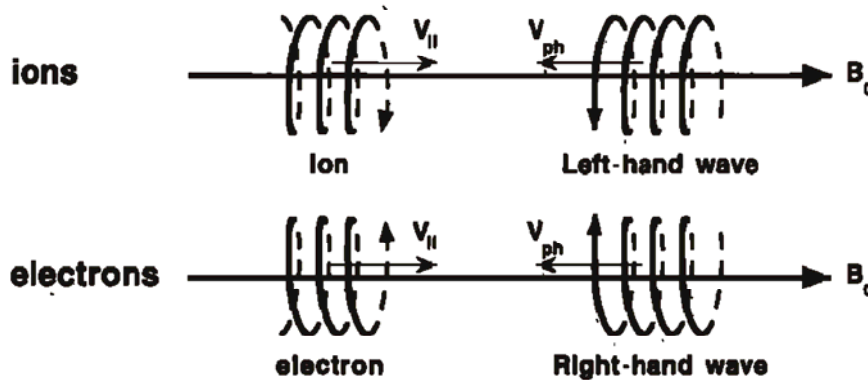


Figure 2. For normal resonance the relative motion between the wave and particle Doppler shifts the wave up to the cyclotron frequency of the particle. Image adapted from [4].

Recent Observations of Precipitation

Radiation belt electron losses can be profitably studied from a stratospheric balloon platform [5]. Precipitating electrons scatter electromagnetically from atmospheric atomic nuclei, and the resulting bremsstrahlung x-radiation penetrates, with little loss, to near 30 km, an altitude readily accessible to balloons. While electron energy and temporal features are reliably inferred from the recovered x-ray spectra, electron pitch angle information is lost, excepting that loss cone electrons alone contribute to x-ray production. As with ground-based observations of radiation belt losses, and unlike space-based observations, balloons are effectively stationary. That is, with stratospheric winds of order 10 m/s, the primary motion of a balloon originates in Earth's spin.

Because extended observations can be collected from a single location, it is possible to study slower low frequency aspects of loss mechanisms. Furthermore, time series from still platforms are purely temporal, exhibiting no confusing component of platform motion through spatial gradients. Because bremsstrahlung production is immediate, and x-rays travel at light speed, the sole time scale introduced by the balloon-bremsstrahlung technique is a delay of order 100 microseconds. Consequently, balloon measurement of radiation belt electron precipitation can span the time range 10^{-4} to 10^4 seconds.

The BARREL project was conceived to augment the Radiation Belt Storm Probe (RBSP) mission, by providing an extended and extensive observation of radiation belt losses to the atmosphere. The RBSP spacecraft, renamed Van Allen probes, cannot accurately measure fluxes inside the small equatorial loss cone. The absence of loss measurements strongly limits one's ability to connect losses with in situ observations of particle fluxes and wave spectra. BARREL achieves extensive observations by employing multiple stratospheric platforms at once. The polar vortex and a staggered launching schedule together confer a local time separation between balloons. Payloads were launched from two Antarctic sites to provide L-shell spread (i.e., a spread in geomagnetic latitude), and to reduce risks from logistical or surface weather problems. BARREL achieves extended observations through two campaign periods, the Antarctic summers of 2013 and 2014, with up to 40 instruments deployed altogether, and an average data collection time of about 8 days per balloon. The launch bases were chosen to immediately position balloons where radiation belt electron loss flux measurements are most probable [6]. Figure 3 shows flight paths and altitudes of 5 balloons over a 24 hour period in January 2013. Stratospheric winds transport the balloons westward from their launch sites, marked as two spots along the upper coastline (constant L-curves are derived from the IGRF model). Altitude is important, because the amount of atmosphere between the x-ray source and the detector varies diurnally. The lower panel shows that altitude variation is about a scale height, due to near constant sunlight during the campaign period.

The accumulated dataset from BARREL is used to identify and characterize radiation belt losses. For example, Figure 4 shows x-ray spectrograms during the same 24 hour period of Figure 3. Annihilation radiation at

511 keV produces the horizontal band at the top of each panel. Flux variations extend throughout the depicted energy range of 50-550 keV at 3 of the 5 balloons, but only in the L=4.5-6.5 range. Therefore, electrons of energy exceeding 500 keV were lost to the atmosphere on this day. The x-ray differential energy spectra can be inverted into electron spectra to quantify those losses. Episodes of elevated precipitation are seen to last for order 10 minutes and occur several times. Episodes can extend over 6 hrs of magnetic local time, for instance, at 14:30; although most episodes exhibit smaller spatial extent. These measurements will become even more useful when combined with data from the Van Allen probes.

While difficult to observe from spacecraft, low frequency modulation (Pc-4 to Pc-5, or several minutes period) of radiation belt precipitation is sometimes observed from balloon platforms [7]. These modulation frequencies are well below those of the electromagnetic ion cyclotron or whistler modes, the modes regarded by many as responsible for pitch-angle scattering electrons into the loss cone. Hence the low frequency observations have stimulated recent theoretical work to understand the role of low frequency waves in loss processes [8]. The main idea investigated in this recent simulation work is that magnetic field compressional variation lowers the mirroring altitude, resulting in loss. Results compared well with balloon-borne x-ray measurements. Much work remains to be done in investigating the role of Pc4/Pc5 waves and radiation belt electron losses.

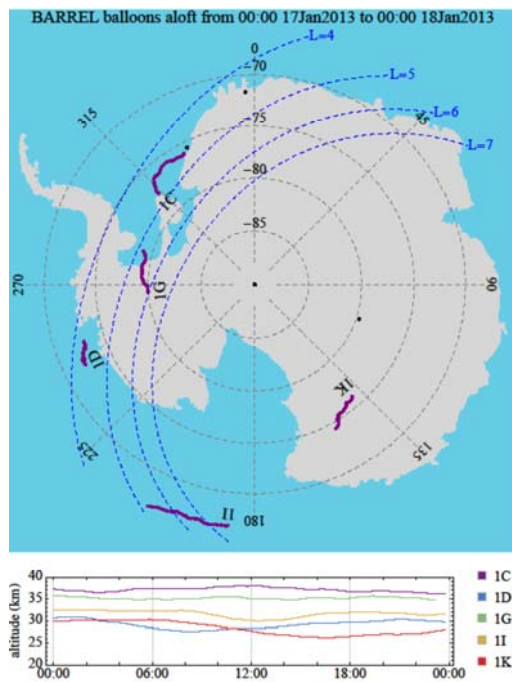


Figure 3. Upper panel shows positions of five balloon payloads over a 24 hour interval; dots mark the two launch sites and the geomagnetic pole. Circumpolar winds move balloons westward in magnetic latitude and longitude. Together with the two launch sites, these winds endow an L-shell and local time extent to the array. Lower panel shows that balloon altitude, though relatively constant over a day, varies as much as a pressure scale height.

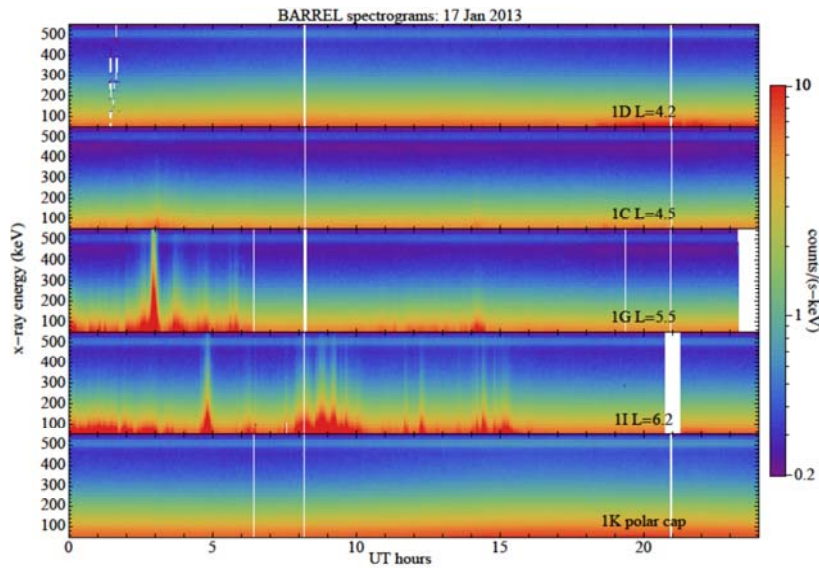


Figure 4. Simultaneous x-ray spectrograms from five payloads show different features due to different geomagnetic locations. In the polar cap (bottom panel), there is no flux change, and therefore no variation in energetic electron precipitation. At lower L-shell (middle panels), there are multiple intervals of electron precipitation, to several hundred keV energy, during this day. Enhanced electron precipitation, below 100 keV, is seen as low as L=4.2 (top panel). The faint band at 511 keV in all spectrograms is the positron annihilation line, which is used as an absolute calibration source.

Recent Advances in Theory Describing Precipitation

Recently, it has been shown that the anomalous cyclotron resonance between relativistic electrons and EMIC triggered emissions [9, 10] takes place very effectively near the magnetic equator because of the rising-tone frequency (Figure 5a) and the variation of the ambient magnetic field. Efficient precipitation is caused by nonlinear trapping of relativistic electrons by electromagnetic wave potentials formed by EMIC triggered emissions. Frequency sweep rates of rising-tone emissions and the inhomogeneous magnetic field play essential roles in the nonlinear trapping of resonant electrons, transferring them to lower pitch angles [11]. The necessary conditions of the wave amplitude, kinetic energies, and pitch angles that must be satisfied for the nonlinear wave trapping have recently been derived. This has led to test particle simulations with a large number of relativistic electrons undergoing mirror motion in a parabolic magnetic field near the magnetic equator [12]. In the presence of coherent EMIC triggered emissions with increasing frequencies, a substantial amount of relativistic electrons are trapped by the wave, and the relativistic electrons at high pitch angles are guided to lower pitch angles within a short time scale much less than a second (Figure 5b), resulting in rapid precipitation of relativistic electrons or relativistic electron microbursts (Figure 5c). Up to this point, it has been widely assumed that relativistic electron microbursts were caused by whistler mode chorus elements, although the observed relativistic electron microbursts energy signature was inconsistent with that expected from chorus [13]. It seems possible that whistler mode chorus may cause some fraction of relativistic electron microbursts [14], especially those seen on the dayside [16]. Nonetheless, the new theoretical understanding may help explain the apparent inconsistency, while also giving greater importance to the role of EMIC waves. The arrival of observations from the Van Allen Probes are also allowing EMIC-driven scattering to be examined in a new light [16].

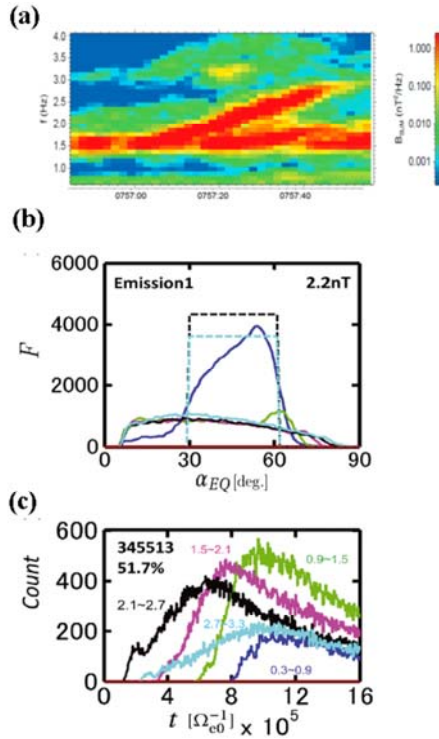


Figure 5. (a) EMIC triggered emissions observed by the Cluster spacecraft [9, 10]. (b) Equatorial pitch angle distribution functions of trapped relativistic electrons (solid lines) after interaction with EMIC triggered emissions, and (c) numbers of precipitating electrons of different energy ranges of 0.3-0.9, 0.9-1.5, 1.5-2.1, 2.1-2.7, and 2.7, 3.3 MeV in blue, green, magenta, black, and cyan, respectively (results of test particle simulations with the initial uniform distributions 30-60 degrees by dashed lines) [12].

EMIC Observations

As noted above, Electromagnetic Ion Cyclotron (EMIC) waves are able to resonate with ring current ion populations as well as relativistic electrons causing pitch angle scattering into Earth's atmosphere. Recent experimental studies have shown EMIC wave growth occurs at all local times and can persist for hours and sometimes even days [17, 18]. With such longevity and broad growth regions, the potential for EMIC waves to be an important cause of radiation belt particle loss increases. With an array of satellite instrumentation including the Van Allen Probes, GOES, and POES in conjunction with BARREL balloons and ground based instruments, have allowed new insights into the spatial and temporal extent of EMIC waves, the propagation from the generation region to satellites and ground instruments, and particle loss processes resulting from interactions with ions and electrons [19]. Figure 6 shows an example of the widespread nature of the EMIC waves and the concurrent precipitation of electrons. EMIC waves are detected simultaneously for about two hours across at least five hours of MLT on the nightside magnetosphere and cover about 4 L-shells. Additional data, not shown here, increases the range in MLT to at least 12 hours of MLT. This significantly expands the MLT range reported in previous studies. For example, a recent examination of large scale EMIC wave precipitation using ground based aurora cameras to examine the EMIC precipitated protons concluded this was occurring over ~ 4 hours of MLT [20], emphasising the need for global observations to determine the true spatial size.

These new observational studies are calling into question the current under-standing of EMIC waves being detected primarily in the dusk region and the conditions under which the waves can be generated. Experimental observations indicate that the temporal and spatial range of the generation region appears to be much larger than has been previously suggested studies [17]. In addition, Antarctic ground-based observations show that EMIC waves occur more often and are detected at higher frequencies (>1 Hz), contrary to previous studies stating EMIC waves

peak at solar minimum. It appears that increased solar activity is driving temperature anisotropies closer to Earth (at larger magnetic field strength), thus elevating the wave frequency [21]. A number of recent studies call into question the canonical understanding of EMIC waves and their understanding to the precipitation of relativistic electrons from the radiation belts. Several theoretical and modelling studies have predicted EMIC wave driven electron precipitation through pitch angle scattering into the loss cone [22], but it has only been in the last few years that direct evidence of this interaction has been detected [23, 24]. An area of active research concerns how much of an impact the EMIC waves make on the radiation belts when they are able to resonate with the relativistic electrons.

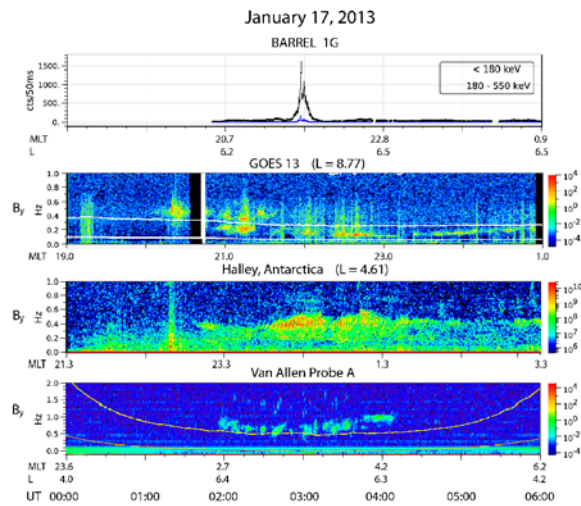


Figure 6. Data from BARREL balloon 1G, GOES 13, Halley, Antarctica, and Van Allen Probe A on 17 January 2013. The BARREL balloon data shows counts per 50 ms of Bremsstrahlung x-rays from which electron precipitation is inferred. The next three plots show magnetometer data with the helium and oxygen cyclotron frequencies superimposed on the GOES and Van Allen Probe plots. The proton cyclotron frequency is above the range of the plots.

Low-Energy Precipitation as a Proxy for Whistler Mode Waves

In the last year, a new approach has been put forward using comparatively low-energy precipitation (tens of keV) observations in an exciting innovative way. As noted above, whistler mode waves resonate with electrons over a wide energy range leading to precipitation. Thus, one can use precipitation as a proxy for the wave activity.

Whistler-mode chorus waves have received intense attention recently due to the important dual role they play in acting both as loss and acceleration processes for energetic electrons [25]. Since chorus-driven electron scattering and energization is fundamentally important for radiation belt electron dynamics, it is crucial to understand the global evolution of chorus wave intensity. Although statistical chorus wave distributions were previously used to simulate radiation belt electron dynamics during a geomagnetic storm, chorus wave distributions from statistical results may not accurately represent the true, instantaneous global wave evolution in a particular event.

Low-altitude electron measurements by multiple POES satellites have been used in a recent study to infer whistler-mode chorus wave amplitudes using a physics-based technique [26]. POES satellites have two particle detectors, which can measure both precipitated and trapped electron fluxes [27], and multiple satellites are distributed in a broad MLT region to provide extensive coverage in both L-shell and MLT. Quasi-linear theory [28] and the UCLA full diffusion code [29] are applied to quantify the electron scattering process near the loss cone driven by chorus waves, and the ratio of precipitated and trapped electron fluxes, in turn, is used to infer chorus wave amplitudes [26]. This technique has been validated by analyzing conjunction events between the Van Allen Probes measuring chorus wave amplitudes near the equator and POES satellites measuring the 30-100 keV electron population at the conjugate low altitudes.

This technique was used to construct the global distribution of chorus wave intensity as a function of L-shell in various MLT ranges during a double dip storm, which occurred during 07-10 October in 2012 (Figure 7). The precipitated (Figure 7c) and trapped electron fluxes (Figure 7d), and their ratio (Figure 7e), increase during the double dips in SYM-H. The chorus wave amplitudes inferred from the ratio of precipitated and trapped electron fluxes over 03-09 MLT (Figure 7f) agree well with the conjugate measurements of chorus wave amplitudes from the Van Allen Probes (Figure 7b) in the similar MLT sector. The evolution of the whistler-mode wave intensity inferred from low-altitude electron measurements can provide real-time global estimates of the wave intensity over a broad L-MLT region (Figure 7f-7i), which cannot be obtained from in-situ wave measurements by equatorial satellites alone, but is crucial in quantifying radiation belt electron dynamics.

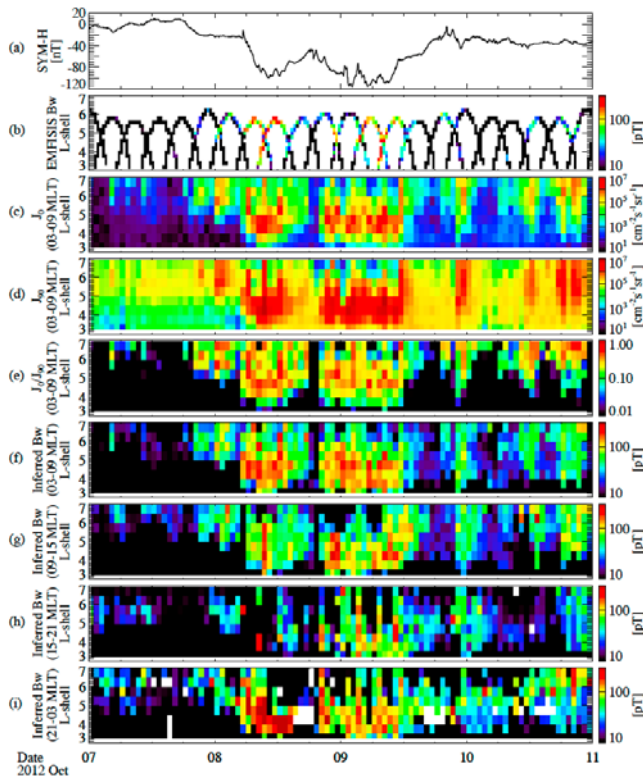


Figure 7. Evolution of whistler-mode chorus wave intensity measured by Van Allen Probes and low-altitude electron measurements by multiple POES satellites during 07-10 October 2012. (a) Sym-H index, (b) chorus wave amplitudes integrated over $0.1 - 0.5 f_{ce}$ measured by the EMFISIS instruments on both Van Allen Probes A and B, where f_{ce} is the equatorial electron cyclotron frequency. (c) Precipitated electron flux (J_p), (d) trapped electron flux (J_0), and (e) the ratio of J_p/J_0 in the 30-100 keV energy channel near the dawn sector over 03-09 MLT measured by multiple POES satellites. (f)-(i) inferred chorus wave intensity from the ratio of precipitated and trapped electron fluxes in various MLT ranges.

Precipitation Affecting the Wider Earth System

Due to the Earth's magnetic field configuration, energetic particle precipitation occurs mainly in the polar auroral and sub-auroral regions, i.e., at latitudes higher than 45° . The altitudes at which these particles deposit their momentum is dependent on their energy spectrum, with lower energy particles impacting the atmosphere at higher altitudes and higher energy particles penetrating more deeply. Precipitating charged particles produce NO_x ($\text{NO}_x = \text{NO} + \text{NO}_2$) and HO_x ($\text{HO}_x = \text{OH} + \text{HO}_2$) through ionization or dissociative ionization of N_2 and O_2 molecules, which results in the formation of N^+ , O^+ , N^+ , O^+ , and NO^+ . Energetic particle precipitation has been observed to

cause significant increases in NO_x and HO_x in the polar atmosphere [30, 31, 32]. These chemicals are particularly important in that they catalytically destroy ozone [33].

There has also been growing evidence that geomagnetic storms produce high fluxes of energetic electron precipitation [34], with modelling suggesting energetic electron precipitation can also lead to significant mesospheric chemical changes in the polar regions [35] affecting the chemical makeup of the polar atmosphere. The radiative balance of the atmosphere is driven by its composition, particularly through the abundance of ozone and its capability of absorbing solar UV radiation efficiently [33]. As NO_x and HO_x influence the ozone abundance at upper stratosphere and mesospheric levels, the radiative balance can be altered and temperature gradients are modified. Through this mechanism atmospheric wind patterns can be altered, influencing the propagation of planetary and gravity waves within the stratosphere and troposphere. As Figure 8 shows, this step-by-step process provides a pathway to link geomagnetic storm perturbations in the radiation belts, with chemical changes in the upper atmosphere, and ultimately, with the dynamics of the lower atmosphere.

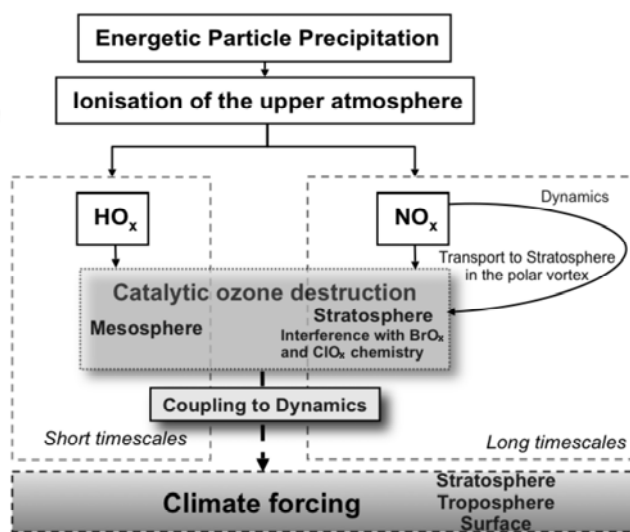


Figure 8. A schematic of the effects of energetic particle precipitation into the upper atmosphere, flowing down through the stratosphere to effect tropospheric climate.

References

1. C. J. Rodger, and M. A. Clilverd, Magnetospheric Physics: Hiss from the Chorus, *Nature*, 452 (7183), 41-42, doi:10.1038/452041a, 2008.
2. L. R. Lyons, and R. M. Thorne, Parasitic Pitch Angle Diffusion of Radiation Belt Particles by Ion Cyclotron Waves, *J. Geophys. Res.*, 77(28), 5608–5616, doi:10.1029/JA077i028p05608, 1972
3. R. M. Thorne, Radiation belt dynamics: The Importance of Wave-Particle Interactions, *Geophys. Res. Lett.*, 37, L22107, doi:10.1029/2010GL044990, 2010.
4. B. T. Tsurutani, and G. S. Lakhina, Some Basic Concepts of Wave-Particle Interactions in Collisionless Plasmas, *Rev. Geophys.*, 35(4), 491–501, doi:10.1029/97RG02200, 1997.
5. G. K. Parks, T. J. Freeman, M. P. McCarthy, and S. H. Werden, The Discovery of Auroral X-Rays by Balloon-Borne Detectors and Their Contributions to Magnetospheric Research, in *Auroral Plasma Dynamics* (ed R. L. Lysak), American Geophysical Union, Washington, D. C., doi: 10.1029/GM080p0017, 1993.

6. R. M. Millan, M. P. McCarthy, J. G. Sample, D. M. Smith, L. D. Thompson, D. G. McGaw, L. A. Woodger, J. G. Hewitt, M. D. Comess, K. B. Yando, A. X. Liang, B. A. Anderson, N. R. Knezek, W. Z. Rexroad, J. M. Scheiman, G. S. Bowers, A. J. Halford, A. B. Collier, M. A. Clilverd, R. P. Lin, and M. K. Hudson, The Balloon Array for RBSP Relativistic Electron Losses (BARREL), *Space Sci. Rev.*, doi 10.1007/s11214-013-9971-z, 2013.
7. J. E. Foat, R. P. Lin, D. M. Smith, F. Fenrich, R. Millan, I. Roth, K. R. Lorentzen, M. P. McCarthy, G. K. Parks, and J. P. Treilhou, First detection of a Terrestrial MeV X-ray Burst, *Geophys. Res. Lett.*, vol 25, DOI: 10.1029/1998GL900134, 1998.
8. T. Brito, L. Woodger, M. Hudson, and R. Millan, Energetic Radiation Belt Electron Precipitation Showing ULF Modulation, *Geophys. Res. Lett.*, vol 39, doi:10.1029/2012GL053790, 2012.
9. J. S. Pickett et al., Cluster Observations of EMIC Triggered Emissions in Association with Pc1 Waves Near Earth's Plasmapause, *Geophys. Res. Lett.*, 37, L09104, 2010.
10. Y. Omura, J. Pickett, B. Grison, O. Santolik, I. Dandouras, M. Engebretson, P. M. E. Décréau, and A. Masson, Theory and Observation of Electromagnetic Ion Cyclotron Triggered Emissions in the Magnetosphere, *J. Geophys. Res.*, 115, A07234, 2010.
11. Y. Omura, and Q. Zhao, Nonlinear Pitch-Angle Scattering of Relativistic Electrons by EMIC Waves in the Inner Magnetosphere, *J. Geophys. Res.*, 117, A08227, 2012.
12. Y. Omura, and Q. Zhao, Relativistic electron microbursts due to nonlinear pitch-angle scattering by EMIC triggered emissions, *J. Geophys. Res.*, doi:10.1002/jgra.50477, 2013.
13. C. J. Rodger, M. A. Clilverd, D. Nunn, P. T. Verronen, J. Bortnik, and E. Turunen, Storm-Time Short-Lived Bursts of relativistic Electron Precipitation Detected by Subionospheric Radio Wave Propagation, *J. Geophys. Res.*, 112, A07301, doi:10.1029/2007JA012347, 2007.
14. T. P. O'Brien, K. R. Lorentzen, I. R. Mann, N. P. Meredith, J. B. Blake, J. F. Fennell, M. D. Looper, D. K. Milling, and R. R. Anderson, Energization of Relativistic Electrons in the Presence of ULF Power and MeV Microbursts: Evidence for Dual ULF and VLF Acceleration, *J. Geophys. Res.*, 108, 1329, doi:10.1029/2002JA009784, 2003.
15. S. Saito, Y. Miyoshi, and K. Seki, Relativistic Electron Microbursts Associated With Whistler Chorus Rising Tone Elements: GEMSIS-RBW Simulations, *J. Geophys. Res.*, 117, A10206, doi:10.1029/2012JA018020, 2012.
16. M. E. Usanova, et al., Effect of EMIC Waves On Relativistic and Ultrarelativistic Electron Populations: Ground-Based and Van Allen Probes Observations, *Geophys. Res. Lett.*, 41, 1375–1381, doi:10.1002/2013GL059024, 2014.
17. C. E. Weaver, M. R. Lessard, J. L. Gannon, M. J. Engebretson, C. J. Farrugia, and V. Pilipenko, Persistent Occurrence of EMIC waves Around Magnetic Noon After a High Speed Solar Stream, *AGU Fall Meeting Abstracts*, page B2112, December 2011.
18. K. W. Paulson, C. W. Smith, M. R. Lessard, M. J. Engebretson, R. B. Torbert, and C. A. Kletzing, In Situ Observations of Pc1 Pearl Pulsations by the Van Allen Probes, *Geophys. Res. Lett.*, 41, doi:10.1002/2013GL059187, 2014.
19. C. E. Weaver, M. R. Lessard, M. J. Engebretson, R. M. Millan, A. Halford, R. B. Horne, H. J. Singer, and J. C. Green, Ground and Satellite EMIC Wave Observations in Conjunction with BARREL Electron Precipitation, *AGU Fall Meeting Abstracts*, 2013.
20. K. Sakaguchi, Y. Miyoshi, E. Spanswick, E. Donovan, I. R. Mann, V. Jordanova, K. Shiokawa, M. Connors, and J. C. Green, Visualization of the Visualization of Ion Cyclotron Wave and Particle Interactions in the Inner Magnetosphere via THEMIS-ASI Observations, *J. Geophys. Res.*, 117, A10204, doi:10.1029/2012JA018180, 2012.

21. C. E. Weaver, E. Lindgren, M. R. Lessard, and M. J. Engebretson, Observations of Increasing EMIC Waves Frequency With the Increasing Solar Cycle, *AGU Fall Meeting Abstracts*, 2012.
22. D. Summers, and R. M. Thorne, Relativistic Electron Pitch-Angle Scattering by Electromagnetic Ion Cyclotron Waves During Geomagnetic Storms, *J. Geophys. Res.*, 108, 1143, doi:10.1029/2002JA009489, A4, 2003.
23. C. J. Rodger, T. Raita, M. A. Clilverd, A. Seppälä, S. Dietrich, N. R. Thomson, and T. Ulich, Observations of Relativistic Electron Precipitation From the Radiation Belts Driven by EMIC Waves, *Geophys. Res. Lett.*, 35, L16106, doi:10.1029/2008GL034804, 2008.
24. Y. Miyoshi, K. Sakaguchi, K. Shiokawa, D. Evans, J. Albert, M. Connors, and V. Jordanova, Precipitation of Radiation Belt Electrons by EMIC Waves, Observed From Ground and Space, *Geophys. Res. Lett.*, 35, L23101, doi:10.1029/2008GL035727, 2008.
25. R. M. Thorne, et al., Rapid Local Acceleration of relativistic Radiation Belt Electrons by Magnetospheric Chorus, *Nature*, 504, 411-414, doi:10.1038/nature12889, 2013.
26. W. Li, B. Ni, R. M. Thorne, J. Bortnik, J. C. Green, C. A. Kletzing, W. S. Kurth, and G. B. Hospodarsky, Constructing the Global Distribution of Chorus Wave Intensity Using Measurements of Electrons by the POES Satellites and Waves by the Van Allen Probes, *Geophys. Res. Lett.*, 40, 4526–4532, doi:10.1002/grl.50920, 2013.
27. C. J. Rodger, M. A. Clilverd, J. C. Green, and M. M. Lam, Use of POES SEM-2 Observations to Examine Radiation Belt Dynamics and Energetic Electron Precipitation into the Atmosphere, *J. Geophys. Res.*, 115, A04202, doi:10.1029/2008JA014023, 2010.
28. C. F. Kennel, and H. E. Petschek, Limit on Stably Trapped Particle Fluxes, *J. Geophys. Res.*, 71(1), 1–28, doi:10.1029/JZ071i001p00001, 1966.
29. B. Ni, R. M. Thorne, Y. Y. Shprits, and J. Bortnik, Resonant Scattering of Plasma Sheet Electrons by Whistler-Mode Chorus: Contribution to Diffuse Auroral Precipitation, *Geophys. Res. Lett.*, 35, L11106, doi:10.1029/2008GL034032, 2008.
30. D. A. Newnham, P. J. Espy, M. A. Clilverd, C. J. Rodger, A. Seppälä, D. J. Maxfield, P. Hartogh, C. Straub, K. Holmén, and R. B. Horne, Observations Of Nitric Oxide in the Antarctic Middle Atmosphere During Recurrent Geomagnetic Storms, *J. Geophys. Res.*, 118, 7874–7885, doi:10.1002/2013JA019056, 2013.
31. Y. Isono, A. Mizuno, T. Nagahama, Y. Miyoshi, T. Nakamura, R. Kataoka, M. Tsutsumi, M. Ejiri, H. Fujiwara, and H. Maezawa, Variations of Nitric Oxide in the Mesosphere and Lower Thermosphere Over Antarctica Associated With a Magnetic Storm in April 2012, *Geophys. Res. Lett.*, 41, doi:10.1002/2014GL059360, 2014.
32. M. E. Andersson, P. T. Verronen, S. Wang, C. J. Rodger, M. A. Clilverd, and B. R. Carson, Precipitating Radiation Belt Electrons and Enhancements of Mesospheric Hydroxyl During 2004–2009, *J. Geophys. Res.*, 117, D09304, doi:10.1029/2011JD017246, 2012.
33. G. P. Brasseur, and Solomon, S., *Aeronomy of the Middle Atmosphere* (3rd revised and enlarged edn), Springer, Dordrecht, 2005.
34. C. J. Rodger, M. A. Clilverd, N. R. Thomson, R. J. Gamble, A. Seppälä, E. Turunen, N. P. Meredith, M. Parrot, J.-A. Sauvaud, and J.-J. Berthelier, Radiation Belt Electron Precipitation Into the Atmosphere: Recovery From a geomagnetic Storm, *J. Geophys. Res.*, 112, A11307, doi:10.1029/2007JA012383, 2007.
35. C. J. Rodger, M. A. Clilverd, A. Seppälä, N. R. Thomson, R. J. Gamble, M. Parrot, J.-A. Sauvaud, and T. Ulich, Radiation Belt Electron Precipitation due to Geomagnetic Storms: Significance to Middle Atmosphere Ozone Chemistry, *J. Geophys. Res.*, 115, A11320, doi:10.1029/2010JA015599, 2010.